Title

OH reactivity in urban and suburban regions in Seoul, South Korea – an East Asian megacity in a rapid transition

Authors

Kim, Saewung
Sanchez, Dianne
Wang, Mark
et al.

Publication Date

2016-07-18

DOI

10.1039/c5fd00230c

Faraday Discussions

Cite this: *Faraday Discuss.*, 2016, **189**, 231

PAPER

OH reactivity in urban and suburban regions in Seoul, South Korea – an East Asian megacity in a rapid transition

Saewung Kim,*[a] Dianne Sanchez,[a] Mark Wang,[a] Roger Seco,[a] Daun Jeong,[a] Stacey Hughes,[b] Barbara Barletta,[b] Donald R. Blake,[b] Jinsang Jung,[c] Deugsoo Kim,[d] Gangwoong Lee,[e] Meehye Lee,[f] Joonyoung Ahn,[g] Sang-Deok Lee,[g] Gangnam Cho,[g] Min-Young Sung,[g] Yong-Hwan Lee,[g] Dan Bi Kim,[g] Younha Kim,[h] Jung-Hun Woo,[h] Duseong Jo,[i] Rokjin Park,[i] Jeong-Hoo Park,[g] You-Deog Hong[g] and Ji-Hyung Hong[g]

Received 20th December 2015, Accepted 11th February 2016
DOI: 10.1039/c5fd00230c

South Korea has recently achieved developed country status with the second largest megacity in the world, the Seoul Metropolitan Area (SMA). This study provides insights into future changes in air quality for rapidly emerging megacities in the East Asian region. We present total OH reactivity observations in the SMA conducted at an urban Seoul site (May–June, 2015) and a suburban forest site (Sep, 2015). The total OH reactivity in an urban site during the daytime was observed at similar levels (~15 s^{-1}) to those previously reported from other East Asian megacity studies. Trace gas observations indicate that OH reactivity is largely accounted for by NO_X (~50%) followed by volatile organic compounds (VOCs) (~35%). Isoprene accounts for a substantial fraction of OH reactivity among the comprehensive VOC observational dataset (25–47%). In general, observed total OH reactivity can be accounted for by the observed trace gas dataset. However, observed total OH reactivity in the suburban forest area cannot be largely accounted for (~70%) by the trace gas measurements. The importance of biogenic VOC (BVOCs) emissions and oxidations used to evaluate the

[a]*Department of Earth System Science, University of California, Irvine, Irvine CA 92697, USA. E-mail: saewungk@uci.edu; Tel: +1-949-824-4531*
[b]*Department of Chemistry, University of California, Irvine, Irvine CA 92697, USA*
[c]*The Division of Metrology for Quality of Life, Korea Research Institute of Standards and Science, Daejeon, South Korea 34113*
[d]*Department of Environmental Engineering, Kunsan National University, Kunsan, South Korea 573-701*
[e]*Department of Environmental Sciences, Hankuk University of Foreign Studies, Yongin, South Korea 449-791*
[f]*Department of Earth and Environmental Sciences, Korea University, Seoul, South Korea 02841*
[g]*Department of Climate and Air Quality, National Institute of Environmental Research, Incheon, South Korea 22689*
[h]*Division of Interdisciplinary Studies, Konkuk University, Seoul, South Korea 05025*
[i]*School of Earth and Environmental Sciences, Seoul National University, Seoul, South Korea 08826*

impacts of East Asian megacity outflows for the regional air quality and climate contexts are highlighted in this study.

1. Introduction

One of the many consequences of the industrial revolution was urbanization. It was initiated in Europe and has spread out to the U.S. and other parts of the world such as Asia and South America.[1] Accelerating technological breakthroughs since the industrial revolution have brought different natures of environmental problems to different parts of the world.[2] For example, coal powered urban areas with limited emission control technologies in the late 1800s and early 1900s suffered public health issues caused by sulfur and soot pollution. A strong boundary layer inversion event that often happened in winter could trigger a massive smog event. In December of 1952, the Great Smog event in London caused ~100 000 casualties including 4000 premature deaths in only four days.[3,4]

A different type of air pollution was reported in Southern California in the early to mid-1900s. The successful implementation of factory smoke emission controls between 1905 and 1912 could not improve the air quality in the Los Angeles area as the size of the automobile fleet had been exponentially increasing.[4] In 1940, the research community realized that nitrogen oxides ($NO_X = NO + NO_2$) and volatile organic compounds (VOCs) emitted from tail pipes became precursors for photochemical reactions triggered by the intense solar radiation in Southern California to produce ozone and particles in the atmosphere.[5,6] Unique local meteorological and topographical characteristics such as a land-sea breeze pattern and a basin structure worsen the photochemical ozone and particle pollution issues in the Los Angeles basin.[4,7] This well known photochemical smog, also known as Los Angeles type smog, has became an issue in most cities in developing and developed countries as automobile use has increased in the mid to late 20th century.[4]

East Asian countries such as China, Japan, South Korea and Taiwan have emerged as important players in the global economy in the mid to late-20th century. Major economic indices show that this development is in its most mature stage in Japan and in a rapidly growing stage in China. The recent establishment of South Korea as a developed country has led to the implementation of aggressive air pollutant emission abatement policies in the past decade.[8] Geographically, South Korea is adjacent to China across the Yellow Sea. Strong continental outflow events often heavily impact the air quality on the Korean Peninsula.[9] The Seoul Metropolitan Area (SMA), the main urban region in South Korea, is home to 23 million inhabitants, approximately half of the total South Korean population. The majority of the land area (65%) in South Korea is covered by forests.[10] The roles of biogenic volatile organic compounds (BVOCs) from the surrounding forest in the SMA have been extensively discussed in the context of ozone and aerosol formation in both models and measurements. Observational results from Taehwa Research Forest (TRF), 30 km southeast from the Seoul city center indicate that isoprene is the dominant hydroxyl radical sink among the observed reactive gas species.[11–13] A regional model evaluation determined that 30–40% of ozone formation can be accounted for by isoprene photochemistry in the suburban region of the SMA. This suggests that anthropogenic and biogenic interactions need to be addressed when discussing regional air quality issues.[13] Ultra high-resolution regional modeling

studies consistently show that the circulation pattern in the SMA brings isoprene and its oxidation products to the city center, leading to ozone enhancements.[14,15] Multiple reports have highlighted the critical roles of BVOCs in East Asian regional photochemistry. Bao and colleagues[16] presented CMAQ model simulation results indicating ozone enhancements of 20 to 26 ppb due to isoprene photochemistry in the Kinki region, Japan. In China, consistent reports emphasizing the importance of BVOCs over strong anthropogenic influences have been published from the Beijing-Tianjin area,[17] the Shanghai region,[18] and the Pearl River Delta region.[19]

Recently, at least two different analytical techniques have become available to directly constrain total OH reactivity (s^{-1}, reciprocal of OH lifetime) in the atmosphere.[20–22] It has long been suspected that our ability to constrain all the reactive trace gases in the atmosphere is limited, especially for VOCs as many species with different compositions and structural variations with various functional groups are emitted to the atmosphere. There is an estimated 10^4 to 10^5 VOCs in the atmosphere, but this is speculated to be a very conservative assessment, especially in the boundary layer.[23] Direct total OH reactivity observations provide quantitative constraints to this missing fraction, which is called missing OH reactivity. The majority of OH reactivity observations in environments with high BVOC concentrations have reported substantial missing OH reactivity (30–90%).[19,22,24–28] There have been two studies regarding total OH reactivity in East Asian megacity regions – Tokyo, Japan[29,30] and the Pearl River Delta, China.[19] Both observations commonly reported missing OH reactivity and speculated the main sources as unaccounted oxygenated VOCs (OVOCs).

We present total OH reactivity observations collected in the Seoul city center during late spring (May 20th to June 15th) and in the TRF in early fall (September 1st to September 15th) of 2015. Therefore, the observational dataset from the city center provides a good snapshot of photochemical environments with a heavy pollution influence. In contrast, the early fall observations were conducted at the TRF where BVOC photochemistry plays an important role in regional air quality in the aged pollution background. These measurements were conducted as part of the multi-year research initiative Megacity Air Pollution Study (MAPS)-Seoul which is designed to improve the level of understanding of emissions, atmospheric transformation, transport and removal processes over the Korean Peninsula. In 2016, an international collaboration aboard the NASA DC-8 airborne laboratory will take place as part of the KORUS-AQ (Korea-US Air Quality Study) field campaign (https://www.espo.nasa.gov/home/korus-aq/content/KORUS-AQ). This discussion provides an opportunity to critically review the current status of atmospheric reactive gas distributions in the urban and the suburban regions in the SMA. Moreover, as most East Asian megacities are characterized by dense population centers surrounded by rural forests, this case study of the SMA serves as a basis to predict future changes in air quality during the rapid development of East Asia that directly affect anthropogenic emission profiles.

2. Experimental

2.1. Total OH reactivity, auxiliary trace gas and meteorological parameters observations

Total OH reactivity was measured using a comparative reactivity method (CRM) – chemical ionization mass spectrometry (CIMS) which has been previously used to

study urban,[22] clean,[25,31] and pristine[22] field environments. A glass flow reactor (~95 ml) was used which consists of two inlets introducing a mixture of ambient air and pyrrole (5 sccm in 5 ppm ± 5%, Air Liquid LLC) and humidified UHP N_2 (200 sccm) for OH generation *via* photolysis from a UV lamp (UVP LLC, Model 11SC-1). The flow rate in the reactor is maintained at 280 sccm by a MKS mass flow controller (M100B). A volume of 50 sccm is introduced into a custom built H_3O^+–CIMS system.[32] Total OH reactivity of ambient air is then experimentally determined by tracing the pyrrole signal in the reactor. The difference in the pyrrole signal with ambient air and ambient air scrubbed by a catalytic converter (Pt-wool kept at 350 °C) is caused by the competition between pyrrole and reactive gases in the ambient air for reactions with OH. Since OH and pyrrole concentrations are controlled by the experimental setup, the change in reactive gas content in the ambient air is the single variable driving the pyrrole signal change. Calibration was conducted in the field and laboratory using a synthetic air sample using a zero-air flow (1 slpm) with an addition of the NIST traceable standard gases (Airgas) in multiple flow rates to generate multi-point calibration curves. We tested with propane (C_3H_8), propene (C_3H_6), and isoprene (C_5H_8) standards for multi-point calibrations. The results indicate a good linearity ($R^2 = 0.998$) over a wide OH reactivity range from 5 s^{-1} to 100 s^{-1}. We estimate the observational uncertainty as 35% (3 sigma) and the lower limit of detection as 5 s^{-1} (3 sigma). We are currently preparing a separate manuscript with detailed characterizations of the CRM-CIMS instrumentation deployed.

Whole air samples[33] were collected for speciated VOC observations during the spring field campaign in Seoul. It was conducted for 12 days twice a day – in the morning (9:00 to 10:00 local time) and the afternoon (14:00 to 15:00 local time), for a total of 24 samples. Continuous VOC observations were also conducted using a proton transfer reaction-time of flight-mass spectrometer (PTR-ToF-MS, IONICON GmbH) system. The time series data for benzene, toluene, xylene, isoprene and acetone from PTR-ToF-MS indicate that canister sampling time periods are representative in the morning and afternoon as no significant spikes from local sources of these compounds are observed (a separate manuscript is under preparation). The analytical characteristics of other observational parameters including trace gases and meteorological parameters for both the city center and TRF are summarized in Table 1.

2.2. Emission and regional chemistry modeling

For emission analysis the National Institute of Environmental Research/Konkuk University-Comprehensive Regional Emissions inventory for Atmospheric Transport Experiments (NIER/KU-CREATE; CREATE)[34] was used. CREATE is a bottom-up emission inventory framework for Asia jointly developed by the National Institute of Environmental Research of South Korea and Konkuk University. This inventory includes anthropogenic, biogenic and biomass burning emission inventories from 2010, and an emission processing system to generate air quality model-ready gridded, temporally allocated, and chemically speciated emissions. The CREATE anthropogenic emissions were originally developed using the GAINS framework (http://www.gains.iiasa.ac.at/gains), allowing us to project base year (2010) emissions into the future using changing energy/control scenarios. We have used base year anthropogenic emissions for China, Korea, and

Table 1 Analytical characteristics for the trace gas and meteorological observations for the preMAPS campaign

Observables	Manufacturer and model number	Uncertainty	Lower limit of detection
CO	Thermo Scientific 48i TLE	10%	40 ppb
NO_X	Thermo Scientific 42i-TL with a photolysis converter	15%	50 ppt
SO_2	Thermo Scientific 43i-TLE	10%	50 ppt
Ozone	Thermo Scientific 49i	5%	<1 ppb
VOCs	Whole air sample with GC-MS Analysis (at UCI)[a]	1–5%	1–5 ppt
	PTR-ToF-MS[b]	12%	20 ppt
Meteorological parameters	LSI LASTEM meteorological sensors		

[a] More details are described in Colman *et al.*[51] [b] More details are described in Kim *et al.*[12]

Japan, from the CREATE inventory. The VOCs were chemically speciated using the SAPRC chemical mechanism (http://www.engr.ucr.edu/~carter/SAPRC/) and then categorized into alkane, alkene, aromatics and isoprene species. Total emissions were separated by country emissions of CO, NO_X, SO_2, alkane, alkene, aromatics, and isoprene.

Model simulations for the observation periods were conducted using the GEOS-Chem model version v9-02, which was driven by Goddard Earth Observing System-Forward Processing (GEOS-FP) assimilated meteorological data from the NASA Global Modeling and Assimilation Office (GMAO). The GEOS-FP meteorological data have a native horizontal resolution of $0.25^\circ \times 0.3125^\circ$ ($\sim 25 \times 25$ km^2) with 72 vertical pressure levels and 3 h temporal frequency (1 h for surface variables and mixed layer depths). In order to minimize the amount of memory required, we reduced the number of vertical levels to 47 by merging layers in the stratosphere. We use a nested version of GEOS-Chem with the native spatial resolution ($0.25^\circ \times 0.3125^\circ$) over Asia (70°E–140°E, 15°N–55°N). The lateral boundary conditions of the nested model are updated every 3 h from a global simulation at $2^\circ \times 2.5^\circ$ horizontal resolution. Detailed descriptions of gas and aerosol simulations can be found in the literature[35–39]

Biogenic VOC emissions are from the Model of Emissions of Gases and Aerosols from Nature (MEGAN) v2.1 inventory.[40] The emissions of these compounds are calculated on the basis of emission activity factors, canopy environment, leaf age, and soil moisture. Biogenic emissions of isoprene and monoterpenes over nested domains are 1.37 TgC per per month and 0.56 TgC per month, respectively. Anthropogenic emissions in Asia are obtained from the Intercontinental Chemical Transport Experiment Phase B (INTEX-B) inventory,[41] which was compiled on the basis of fuel use statistics for 2006 but scaled to 2015. INTEX-B includes four source sectors: power, industry, residential, and transportation. NO_X and anthropogenic VOC emissions were determined to be 0.62 TgN per month and 1.23 TgC per month, respectively. For biomass burning emissions, we use the Global Fire Emission Database version 3 (GFED v3) inventory for 2011.[42] The GFED inventory is a calculated biogeochemical model

and satellite-derived estimate of area burned, fire activity, and plant productivity. Biomass burning emissions of NO_X and VOCs are 1.7 GgN per month and 5.3 GgC per month, respectively.

2.3. Observational sites

The spring observation was conducted in Korea Institute of Science and Technology (KIST, latitude 37° 36′ 10.4544″ and longitude 127° 2′ 46.0284″). The site is located 5 km northeast of the Seoul city center (Fig. 1). The fall observation is conducted in TRF, 30 km southeast of the Seoul city center, bordering the SMA, and is operated and maintained by the College of Agriculture and Life Sciences at Seoul National University. A trace gas flux tower facility is located in a conifer plantation (*Pinus koraiensis*) surrounded by a natural oak forest where several studies regarding atmospheric composition of the TRF have been conducted.[11–13] The site is under consistent influence from aged Seoul polluted air masses with episodic regional pollution outbreaks from trans-boundary continental pollution outflows. These elevated pollution plumes expedite the photochemical processes of freshly emitted BVOCs. Isoprene has been consistently assessed as the dominant OH sink at the site during the day.[11–13] At night, monoterpenes account for a considerable fraction of OH sinks.[11–13] Unaccounted HONO sources are also highlighted at the site, which may substantially enhance oxidation capacity.[11]

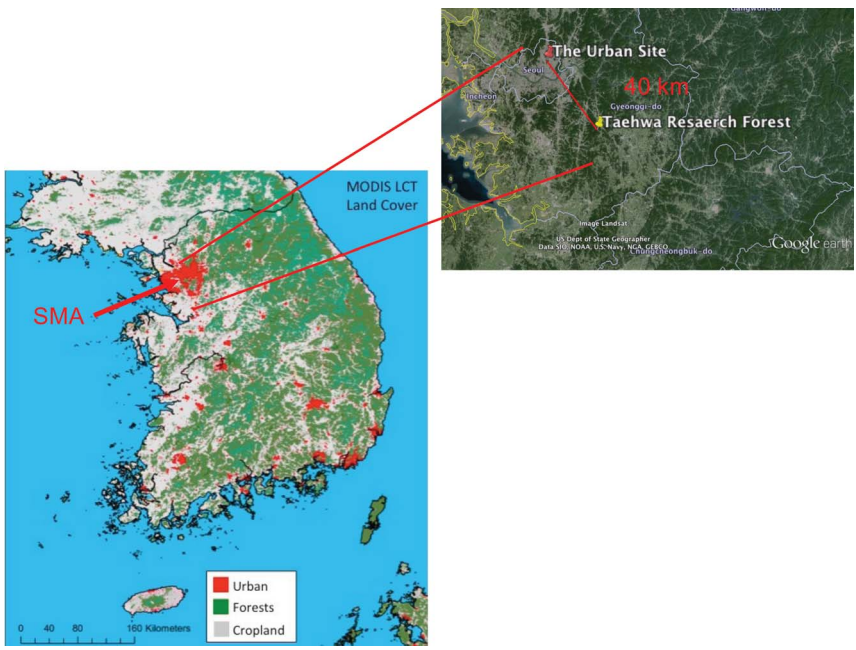

Fig. 1 MODIS (moderate resolution imaging spectroradiometer) land cover types, showing sharp distinction between urban and forested regions. A SMA map indicating the urban site and the suburban forest site (Taehwa Research Forest) is also presented as a subset (photo credit Google Earth).

Table 2 A summary of yearly emissions of anthropogenic trace gases from three East Asian countries in the unit of kmol per year

Countries	NO_X	CO	SO_2	Aromatics	Alkane	Alkene	Isoprene
South Korea	22 948 194.00	90 721 176.00	6 486 774.00	2 415 569.00	4 647 753.00	676 203.00	73 271.00
China	494 421 791.00	5 836 973 662.00	456 185 500.00	66 812 108.00	120 741 973.00	39 753 924.00	919 275.00
Japan	33 984 896.00	159 110 660.00	9 033 697.00	3 629 429.00	6 562 329.00	2 047 176.00	34 990.00

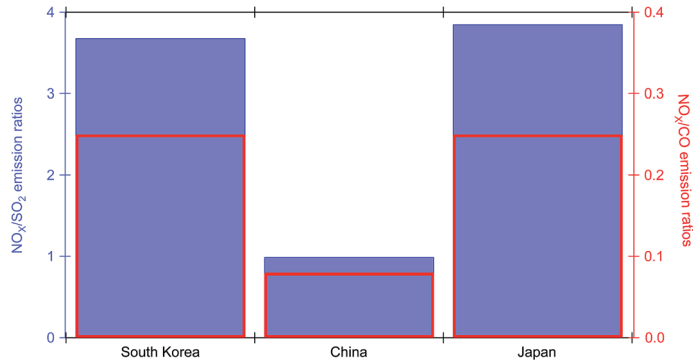

Fig. 2 Emission ratios of NO_X and SO_2 (in blue) and NO_X and CO (in red) assessed for three East Asian countries.

3. Results and discussion

3.1. Trace gas emission profiles

Table 2 summarizes major air pollutant emissions in China, Japan, and South Korea from the CREATE emission inventory. We argue that South Korea exhibits anthropogenic pollutant emissions as an emerging developed country. The ratios of NO_X and SO_2 (Fig. 2) clearly show the anthropogenic trace gas emission profiles in the East Asian countries in different stages of economic development. China shows the lowest ratio and Japan and Korea possess similar ratios. Stricter regulations in coal use become more effective in countries in the more developed stages of economic development such as South Korea and Japan. NO_X emissions from internal combustion engines tend to keep increasing due to increased

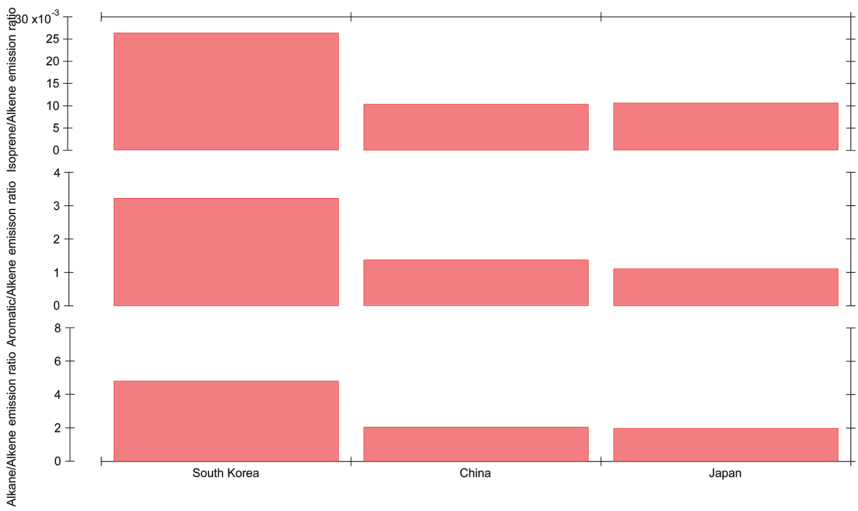

Fig. 3 Emission ratios of VOCs by chemical classes assessed for three East Asian countries.

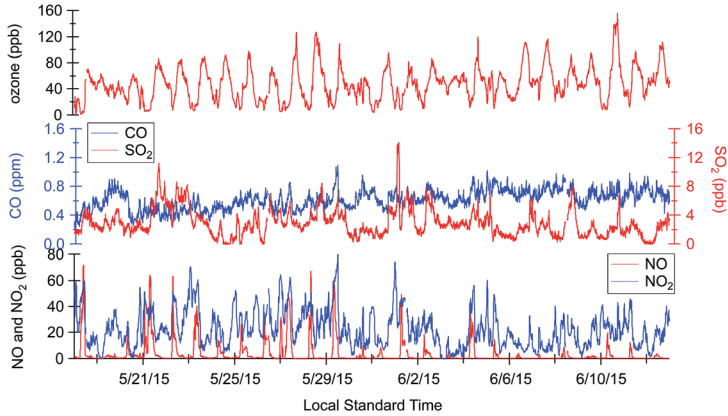

Fig. 4 Time series of observed trace gas variations during the spring campaign in the urban Seoul observational site.

vehicle usage until the economy reaches a mature stage as has been shown in China, Japan, and Korea.[43] In the U.S., several studies integrating satellite NO_X datasets, ground observational networks, and regional photochemical models to assess NO_X emission changes in early 2000 concluded that NO_X emissions have been substantially decreased.[44,45] We can speculate this similar trend may be observable in Japan and Korea in the foreseeable future. In Fig. 2, the NO_X/CO emission ratios are also shown. The highest emission ratio was assessed from Korean emissions. Japan also shows a substantially higher value than that from China. The differences in VOC emission profiles from China, Japan, and Korea can be also highlighted by the ratio of emissions in different chemical classes. Fig. 3 shows the emission ratios of alkane, aromatics and isoprene with alkene. The emission estimates in the CREATE system of alkane, aromatics and isoprene from Korea are all much higher than the alkene emissions.

3.2. Trace gas distributions and total OH reactivity in Seoul

The temporal trace gas variation during the MAPS-Seoul campaign in spring 2015 is shown in Fig. 4. This site has urban characteristics with heavy influences of fresh emissions from traffic. NO_X and CO were at typical levels reported from other air quality monitoring sites in Seoul,[8] which are substantially lower than other megacities such as Beijing,[46,47] Shanghai,[48] and Mexico City[49] (in the 1–2 ppm range) but similar with levels observed in Tokyo.[30] Ambient SO_2 in Seoul is affected by regional transport as the SMA does not have large SO_2 sources and sulfur content in diesel is heavily regulated.[50,51] Indeed, a coal-based Giga power plant cluster is located in the west coast of South Korea ~100 km from Seoul. The back trajectory analysis using the HYSPLIT model frame indicates that the Giga power plant source regions are associated with the enhanced SO_2 levels observed during the field observational period (a manuscript is in preparation). In general, SO_2 is also observed at a much lower level than the levels reported from mega-cities in China[52] (tens of ppb).

In Table 3, the speciated VOCs and their mixing ratio statistics over 12 days are summarized. As the emission inventory suggests, C2 to C4 alkane species were the

Table 3 A summary of observed VOCs with a UCI GC-MS system from canister samples for the 12 day period (24 samples overall) observed at an urban site during the spring campaign

Alkane	Min	Max	Median	Average (STD)	Alkene and alkyne	Min	Max	Median	Average (STD)
Ethane	1814	9620	3325	4143 (2486)	Ethene	245	2694	830	1176 (838)
Propane	532	155 573	2594	4317 (3770)	Ethyne	314	2441	888	1052 (599)
i-Butane	178	5959	1059	1710 (1518)	Propene	44	505	116	190 (150)
n-Butane	316	12 987	1804	3158 (3190)	1-Butene	9	101	23	29 (30)
i-Pentane	181	3431	688	1168 (989)	i-Butene	45	536	95	118 (103)
n-Pentane	126	2315	455	825 (704)	*trans*-2-Butene	7	53	16	20 (13)
n-Hexane	79	1293	329	478 (404)	*cis*-2-Butene	3	34	8	12 (9)
n-Heptane	22	317	98	132 (92)	1,3-Butadiene	5	55	19	23 (15)
n-Octane	12	186	53	68 (52)	1-Pentene	5	67	13	21 (18)
n-Nonane	22	265	72	94 (64)					
n-Decane	21	413	72	104 (89)					
2-Methylpentane	48	711	122	234 (210)					
3-Methylpentane	39	511	99	192 (169)					
2,2,4-Trimethylpentane	22	269	69	98 (75)					
Cyclopentane	17	230	48	85 (71)					
Cyclohexane	21	265	74	101 (76)					

Aromatics	Min	Max	Median	Average (STD)	OVOCs	Min	Max	Median	Average (STD)
Benzene	81	1444	277	324 (282)	Acetaldehyde	960	8927	1823	2351 (1643)
Toluene	798	8926	2035	3093 (2329)	Acetone	6466	21 760	12 041	12 379 (4108)
Ethylbenzene	190	1776	518	698 (474)	Butanal	70	1932	207	303 (127)
p-Xylene	69	834	231	317 (219)	Butanone	329	3096	871	1137 (767)
m-Xylene	87	1405	344	471 (352)	Methanol	3061	31 815	11 140	12 292 (7861)
o-Xylene	63	778	230	321 (211)	Ethanol	783	22 277	3863	6649 (6529)
1,3,5-Trimethylbenzene	3	66	11	18 (18)					
1,2,4-Trimethylbenzene	14	301	41	77 (86)					
1,2,3-Trimethylbenzene	5	105	14	26 (28)					

Table 3 (*Contd.*)

BVOCs	Min	Max	Median	Average (STD)
Isoprene	113	1863	625	690 (408)
Alpha-pinene	7	175	56	76 (53)
Beta-pinene	7	111	24	37 (29)

greatest fraction among the VOCs followed by aromatic compounds. Toluene (~3 ppb) was observed to be 10 times higher than benzene (~0.3 ppb), which is consistent with previous reports from South Korea.[11,13,53] However, in the Beijing-Tianjin area, VOC observations in the summer of 2009 indicate that the ratio of ambient toluene and benzene were observed close to unity.[17] A series of VOC observations in the Tokyo metropolitan area showed a substantially higher toluene level with respect to benzene (5 to 10 times),[29,30] which is consistent with the observational results from Seoul. As benzene and toluene ratios are often used to characterize photochemical age by taking advantage of substantial differences in their reaction constants with OH,[54] the observed near field toluene and benzene ratios would serve as an important constraint to evaluate photochemical aging of the pollution outflows. Acetone and methanol have been observed at high levels in the Beijing-Tianjin metropolitan area[17] and the Tokyo metropolitan area.[29,30] This is also a consistent observation in Seoul. The total sum of VOC mixing ratios is summarized in Fig. 5a. Large differences can be observed among the different chemical classes in the summed mixing ratios. Oxygenated VOCs (OVOCs) and alkane species composed most of the VOC pool.

Once we factor in different reactivity (rate constants[55]) toward OH for each chemical species in Table 3, the relative contributions from different chemical

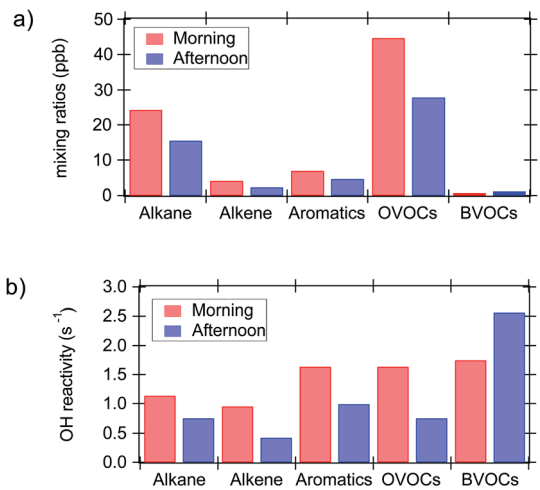

Fig. 5 Averaged (a) concentrations and (b) OH reactivity from different VOC classes during the Seoul urban observations. Morning and afternoon averages are shown in red and blue, respectively.

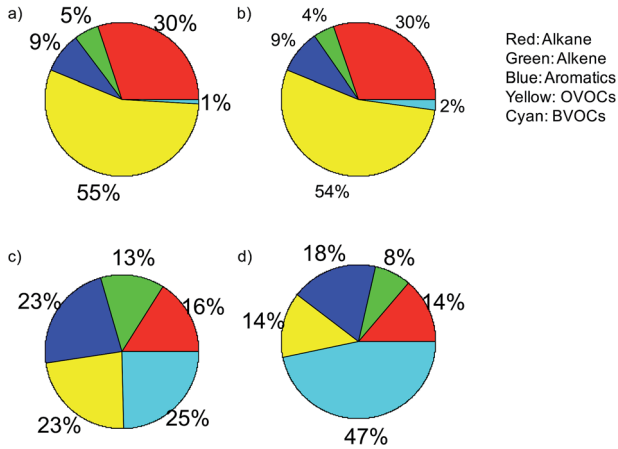

Fig. 6 Relative contributions to mixing ratios from different chemical classes (a) in the morning and (b) in the afternoon and relative contributions to calculated OH reactivity from different chemical classes (c) in the morning and (d) in the afternoon.

classes appear very different from the concentrations (Fig. 5b). Morning contributions to OH reactivity from aromatics, OVOCs and BVOCs primarily from isoprene are evaluated as comparable. BVOCs, again mostly isoprene, are assessed as the dominant OH reactivity contributor in the afternoon. The relative distribution of observed VOCs in the morning and the afternoon are presented in Fig. 6 in both the mixing ratio (Fig. 6a and b) and the OH reactivity scales (Fig. 6c and d). Such a high isoprene contribution (26% in the morning and 36% in the afternoon) to calculated OH reactivity from VOCs in the urban environment has not been commonly reported in the East Asian megacity region. In the suburban regions of the Pearl River Delta,[19] Beijing-Tianjin,[17] and Shanghai,[18] isoprene is an important contributor to OH reactivity. However, in urban environments such as Tianjin and Shanghai, China,[56] isoprene contributes less than ~5% of calculated OH reactivity, and 15% in urban Tokyo, Japan.[29,30] It should be noted that OH reactivity quantitatively represents the roles of chemical species in regional ozone and OVOC production that the concentration scale can often mislead.[57] The dominant contribution to calculated OH reactivity from the ambient observational dataset during the urban observations is from NO_X as shown in Fig. 7. The

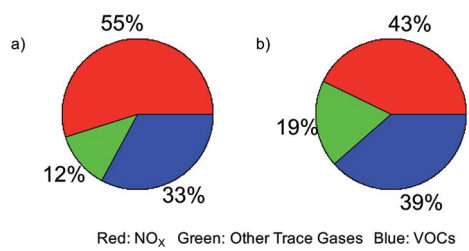

Fig. 7 Relative contributions to OH reactivity from NO_X, other trace gases, and VOCs (a) in the morning and (b) in the afternoon.

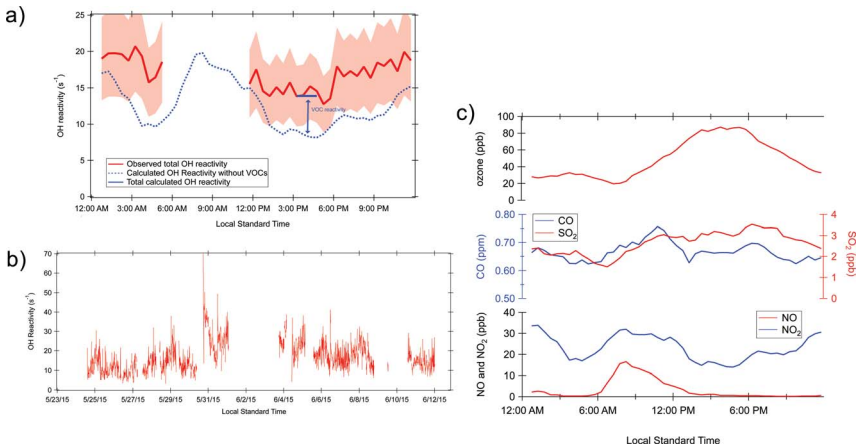

Fig. 8 (a) Averaged diurnal variations in observed OH reactivity, calculated OH reactivity from trace gases without VOCs and total calculated OH reactivity, (b) observed total OH reactivity, and (c) observed trace gas diurnal variation while OH reactivity observation was conducted during the urban observational campaign.

relative contributions from NO_X are significantly higher than those assessed from other East Asian megacities. For example, an observation in Tokyo indicates that NO_X contributes ~35% of calculated OH reactivity.

The averaged diurnal variations of observed and calculated total OH reactivity are shown in Fig. 8a. The average over the 16 days of observations is shown in Fig. 8b. As explained by Sinha and colleagues,[22] the CRM-OH reactivity method systematically underestimates total OH reactivity when NO is higher than 5 ppb

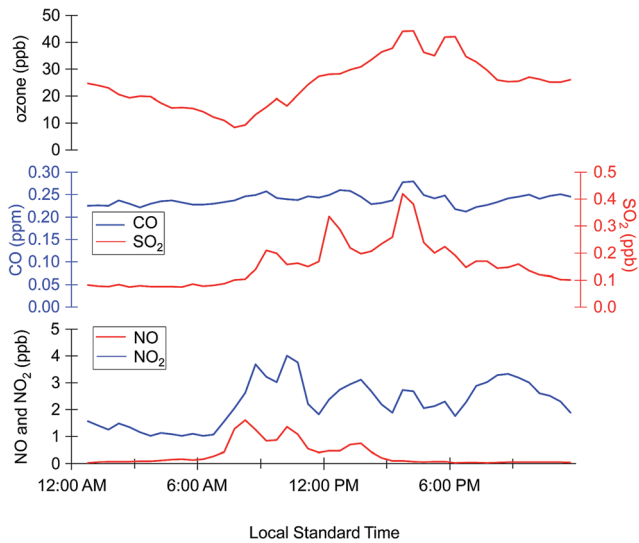

Fig. 9 Observed trace gas diurnal variation while OH reactivity observation was conducted at TRF.

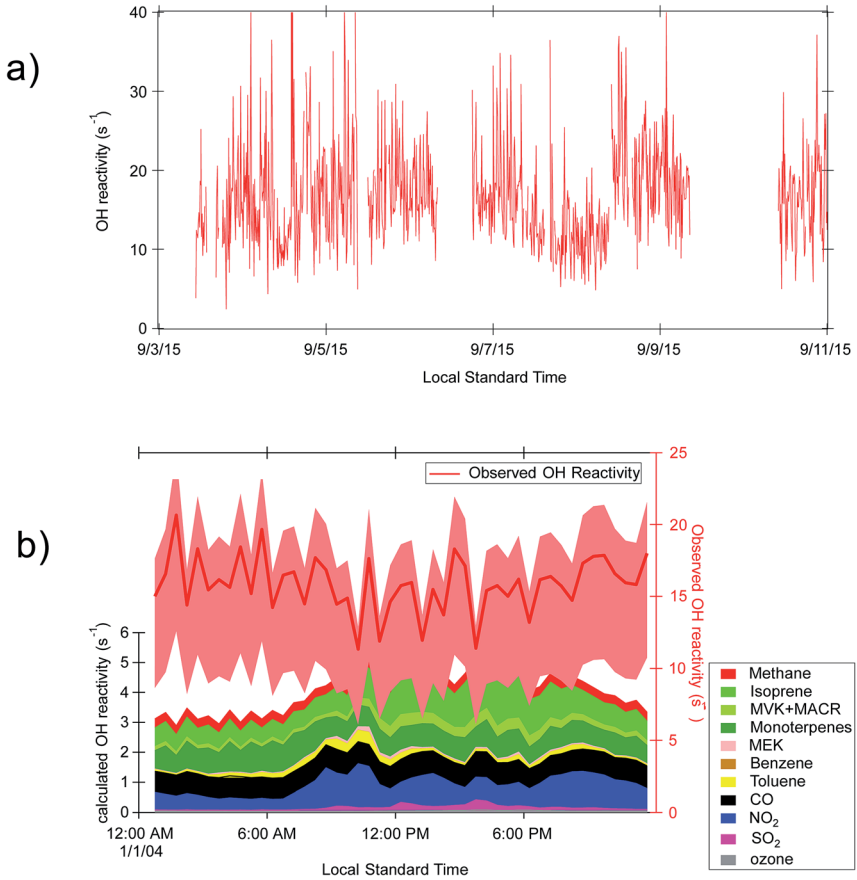

Fig. 10 (a) Observed total OH reactivity and (b) averaged diurnal variations of observed OH reactivity and calculated OH reactivity with a cumulative plot indicating contributions from different observed gas species.

due to fast OH recycling from HO_2. Therefore, total OH reactivity in the morning could not be reported when NO was greater than 5 ppb. Fig. 8c shows the averaged diurnal variations of trace gas observations while the OH reactivity observations were conducted. Despite missing morning data, it is clear that the diurnal variations show higher OH reactivity during the night than observed OH reactivity in the day. Similar results have been reported in the Pearl River Delta region and are most likely attributed to boundary layer evolution, while daytime averages in Seoul are similar to that of Tokyo[29,30], and the Pearl River Delta[19] is comparable. In contrast, the nighttime observed OH reactivity in the Pearl River Delta[19] region was reported to be much higher ($\sim$40 s^{-1})[19] than the observations in the SMA ($\sim$20 s^{-1}). Calculated OH reactivity from trace gases is shown as a dashed blue line in Fig. 8a. Once we add assessed OH reactivity from VOCs observed from the canister samples in the afternoon, the calculated OH reactivity generally accounts for the observed OH reactivity as shown by the blue solid line. This is consistent with the previous OH reactivity observations from urban and megacity environments that have indicated missing OH reactivity smaller than observational uncertainty.

3.3. Trace gas distributions and total OH reactivity in TRF

The September 3–9 trace gas analysis at TRF is presented in Fig. 9. It was consistently sunny during this time period. This rural site located 30 km from the Seoul city center shows a sharp decrease in trace gas concentrations, which is consistent with previous studies,[11–13] and implies fast photochemical processing of megacity pollution plumes. Ultra high-resolution regional model outcomes suggest that the city air pollution plume spreads out to TRF in a time scale of a few hours.[14,15] It should be noted that the sampling was conducted in the late summer/early fall time frame when the regional pollution level is usually much lower than that observed in the spring when the urban observation was conducted. The observed OH reactivity during this time frame is presented in Fig. 10a. Considering the substantially lower pollution levels in this suburban site, significant BVOC influences can be speculated to be the reason. Another noticeable difference from the urban observation is that no strong diurnal pattern could be identified. An identical diurnal trend in OH reactivity was reported from a boreal forest. Sinha and colleagues[25] justified that the observed diurnal variation is most likely caused by the combination of the diurnal boundary layer depth evolution and strong reactive BVOC emission during the daytime. As previously mentioned, air sampling at TRF was conducted in a conifer forest which may provide a plausible explanation of the observed diurnal variation seen in this study. Calculated OH reactivity is assessed based on the trace gas datasets and VOC dataset from PTR-Q(quadrupole)-MS. One of the limitations of PTR-Q-MS for atmospheric VOC quantification is that it cannot quantify most alkane and small alkene ($<C_4$) species. However, previous whole air sample observational results including a comprehensive suite of alkane and alkene species at the TRF have indicated that VOC species that can be quantified by PTR-QMS such as isoprene, toluene, and butanone (methyl ethyl ketone, MEK) account for the majority of VOC contribution towards OH reactivity among atmospheric VOCs.[11,13] Fig. 10b presents the averaged diurnal variation of calculated OH reactivity from the observed trace gas dataset when OH reactivity observation was conducted. The calculated OH reactivity accounts for 30–40% of observed total OH reactivity. Previous studies have reported 30–90% of missing OH reactivity in forested regions with higher missing OH reactivity (50–89%)[25,31] from boreal forests. The

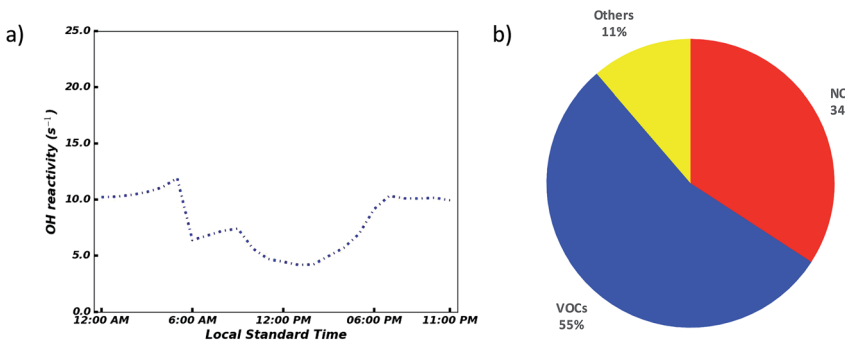

Fig. 11 (a) Simulated diurnal variation of total OH reactivity and (b) relative contributions to simulated OH reactivity from NO_X, other trace gases, and VOCs in Seoul, Korea.

most probable source for missing OH reactivity in forest environments is from either unaccounted BVOC emissions, especially reactive terpenoid species[25,27,31] or unaccounted oxidation products of known BVOCs, specifically isoprene.[19,24,58] In addition, as the roles of extremely low VOCs (ELVOCs) have been recently highlighted in forest canopies with high terpenoid emissions,[59,60] it is a reasonable speculation that ELVOCs which have not been quantified by conventional analytical techniques may contribute towards missing OH reactivity, although the magnitude of their contributions is difficult to assess. Previous observations have indicated that TRF is influenced by both isoprene from deciduous trees from surrounding ecosystems such as oak and mono- and sesquiterpenoids from the conifer tree plantation (200 m by 200 m) near the sampling tower.[11] Therefore, a reasonable assumption can be made that the combination of the different potential sources contributes to missing OH reactivity. Kim and colleagues[11] reported substantial emissions of reactive monoterpenes (α-myrcene) and sesquiterpenes (α and β-caryophyllene) at TRF that have not been quantified in previous studies of branch enclosure measurements. Additionally, the same study highlights potential contributions of unmeasured isoprene oxidation products to the missing OH reactivity (up to 50–70%). More advanced analytical techniques may need to be deployed at this site to qualitatively characterize the sources of missing OH reactivity.

3.4. Comparisons with predicted OH reactivity by a regional modeling system

Fig. 11 shows the diurnal variation of simulated total OH reactivity in the SMA averaged for the MAPS campaign period. Values are much lower than observed or calculated OH reactivity based on the observed species concentrations shown in Fig. 8. The observed high OH reactivity in the night-time and low OH reactivity in the day-time are captured by the model, reflecting the diurnal variation of PBL. However, the pronounced increase of the observed OH reactivity during the night is not captured by the model. The model spatial resolution of about 25 km may still not be fine enough to resolve concentrated pollution plumes from traffic on surrounding highways.

Fig. 11b shows the relative contributions of individual species to the simulated total OH reactivity. The simulated OH reactivity from NO_X is 2.76 s^{-1}, much lower than the observed OH reactivity from NO_X (7.2 s^{-1}), indicating that the model likely underestimates high NO_X concentrations from the traffic in the SMA. We find, however, that the simulated OH reactivity from VOCs is 4.41 s^{-1}, similar to the observed value, 5.3 s^{-1}. As a result, the simulated contribution of NO_X to the OH reactivity in the model is lower (34%) than that of the observation (43–55%), whereas the simulated contribution of VOCs to OH reactivity is high. Among the VOCs in the model, alkanes show the highest contribution to the total OH reactivity, which is different from the observation that isoprene is the most dominant contributor to OH reactivity. Currently, we are working on a separate manuscript to assess the model performances in simulating air quality in the SMA, specifically, detailed comparisons between the model outcomes and the observations. We realize that even a regional photochemical model frame with an enhanced spatial resolution cannot properly capture the photochemical characteristics of TRF, which is located on the border between urban and forest areas. However, the impacts of unconstrained OH reactivity in the suburban forest should be carefully

examined in the perspective of their roles in regional ozone and aerosol formation, which may not be properly represented in the regional modeling system.

4. Summary

Air quality in megacities has been highlighted for its implications towards public health and short lived radiative forcers such as ozone and secondary aerosols.[61] We comprehensively discussed the observed trace gas and total OH reactivity datasets from the SMA. The SMA is the second largest metropolitan area in the world and presents developed pollutant emission profiles among the megacities in East Asia. This case study in the SMA provides an opportunity to test our current understanding of photochemistry in East Asian megacities. Particularly, how atmospheric composition will change in megacities and rapidly evolving energy usage and pollutant emission profiles through an ambitious government driven policy. The city center observation dataset indicates that NO_X accounts for 50% of OH reactivity among the observationally constrained reactive gas species. The NO_X contributions become much higher in the morning (55%) than those in the afternoon (43%). VOC contributions to OH reactivity are followed by NO_X with a greater contribution in the afternoon (39%) than in the morning (33%). In the concentration scales, alkane and OVOCs are the dominant VOC species. However, the importance of BVOCs, particularly isoprene, in urban photochemistry is highlighted by assessing relative contributions to OH reactivity. BVOCs mostly isoprene accounts for 25% of calculated OH reactivity among the observed VOCs in the morning and 47% in the afternoon. In contrast, the BVOC contributions are assessed to be 1% and 2% within the concentration scale, respectively. The observed OH reactivity in late May and early June of 2015 in the SMA city center indicates a similar range to other reported OH reactivity values (10–20 s^{-1}) from Tokyo, Japan[29,30] and Pearl River Delta, China.[19] However, nighttime OH reactivity was observed to be at a much higher level in Pearl River Delta, China. The overall calculated OH reactivity from observed trace gases and VOC species in this campaign account for the greatest fraction of the observed OH reactivity level in the afternoon. However, the observational results from TRF indicate a large missing OH reactivity, as calculated OH reactivity from observed trace gases and VOCs can only account for 24–32% of the total observed OH reactivity. The observed range of missing OH reactivity has been reported in other forest ecosystems where anthropogenic influences are minimal such as a boreal forest in Finland.[22,31] The pollution level in TRF is assessed as substantially lower than the center of Seoul, but the level of air pollutants such as CO and NO_X is still much higher in the TRF than that in the boreal forest. Therefore, how interactions between pollution and BVOCs in photochemistry would affect the formation of oxidation products not quantified by conventional analytical techniques (in our case PTR-Q-MS) should be carefully examined. In addition, potential uncharacterized BVOC emissions in the ecosystem should be carefully characterized. Overall, our presented observational results highlight a significant role of BVOCs in the local photochemical processes in the SMA. As similar land use characteristics – a densely populated urban area surrounded by a forested area – can be found in most megacities in East Asia, our analysis should be able to be applied to characterizing regional photochemical characteristics. Furthermore, several studies have interpreted the significant implications of East Asian air pollution

into the global tropospheric composition influencing the global radiative budget.[62,63] Therefore, enhancing process level understanding of local photochemistry in the East Asian region will be essential in diagnosing and predicting global radiative forcing from short lived climate forcers.[64]

Acknowledgements

This research is supported by National Institute of Environmental Research (NIER) of South Korea.

References

1 UN, *World Urbanization Prospects*, United Nations, New York, New York US, 2014.
2 D. Y. Zhang, J. J. Liu and B. J. Li, *Sustainability*, 2014, **6**, 5322–5338.
3 D. L. Davis, M. L. Bell and T. Fletcher, *Environ. Health Perspect.*, 2002, **110**, A734–A735.
4 M. Z. Jacobson, *Air Pollution and Global Warming-History, Science, and Solutions*, Cambridge University Press, New York, New York U.S., 2012.
5 A. J. Haagen-Smit, *Ind. Eng. Chem.*, 1952, **44**, 1342–1346.
6 F. E. Blacet, *Ind. Eng. Chem.*, 1952, **44**, 1339–1342.
7 J. G. Edinger, *Environ. Sci. Technol.*, 1973, **7**, 247–252.
8 NIER, *Annual Report for Atmospheric Environment*, National Insititute of Environmetal Rsearch, 2010.
9 S. S. Yum, G. Roberts, J. H. Kim, K. Y. Song and D. Y. Kim, *J. Geophys. Res.: Atmos.*, 2007, **112**.
10 Y. J. Lim, A. Armendariz, Y. S. Son and J. C. Kim, *Atmos. Environ.*, 2011, **45**, 2202–2210.
11 S. Kim, S. Y. Kim, M. Lee, H. Shim, G. M. Wolfe, A. B. Guenther, A. He, Y. Hong and J. Han, *Atmos. Chem. Phys.*, 2015, **15**, 4357–4371.
12 S. Kim, M. Lee, S. Kim, S. Choi, S. Seok and S. Kim, *J. Atmos. Sci.*, 2013, **49**, 325–331.
13 S. Y. Kim, X. Y. Jiang, M. Lee, A. Turnipseed, A. Guenther, J. C. Kim, S. J. Lee and S. Kim, *Atmos. Environ.*, 2013, **70**, 447–453.
14 K. Y. Lee, K. H. Kwak, Y. H. Ryu, S. H. Lee and J. J. Baik, *Atmos. Environ.*, 2014, **96**, 209–219.
15 Y. H. Ryu, J. J. Baik, K. H. Kwak, S. Kim and N. Moon, *Atmos. Chem. Phys.*, 2013, **13**, 2177–2194.
16 H. Bao, K. L. Shrestha, A. Kondo, A. Kaga and Y. Inoue, *Atmos. Environ.*, 2010, **44**, 421–431.
17 L. Ran, C. S. Zhao, W. Y. Xu, X. Q. Lu, M. Han, W. L. Lin, P. Yan, X. B. Xu, Z. Z. Deng, N. Ma, P. F. Liu, J. Yu, W. D. Liang and L. L. Chen, *Atmos. Chem. Phys.*, 2011, **11**, 4657–4667.
18 F. Geng, X. Tie, A. Guenther, G. Li, J. Cao and P. Harley, *Atmos. Chem. Phys.*, 2011, **11**, 10449–10459.
19 S. Lou, F. Holland, F. Rohrer, K. Lu, B. Bohn, T. Brauers, C. C. Chang, H. Fuchs, R. Haseler, K. Kita, Y. Kondo, X. Li, M. Shao, L. Zeng, A. Wahner, Y. Zhang, W. Wang and A. Hofzumahaus, *Atmos. Chem. Phys.*, 2010, **10**, 11243–11260.
20 S. Kim, A. Guenther and E. Apel, *Environ. Sci.: Processes Impacts*, 2013, **15**, 1301.

21 T. A. Kovacs and W. H. Brune, *J. Atmos. Chem.*, 2001, **39**, 105–122.
22 V. Sinha, J. Williams, J. N. Crowley and J. Lelieveld, *Atmos. Chem. Phys.*, 2008, **8**, 2213–2227.
23 A. H. Goldstein and I. E. Galbally, *Environ. Sci. Technol.*, 2007, **41**, 1514–1521.
24 P. M. Edwards, M. J. Evans, K. L. Furneaux, J. Hopkins, T. Ingham, C. Jones, J. D. Lee, A. C. Lewis, S. J. Moller, D. Stone, L. K. Whalley and D. E. Heard, *Atmos. Chem. Phys.*, 2013, **13**, 9497–9514.
25 V. Sinha, J. Williams, J. Lelieveld, T. M. Ruuskanen, M. K. Kajos, J. Patokoski, H. Hellen, H. Hakola, D. Mogensen, M. Boy, J. Rinne and M. Kulmala, *Environ. Sci. Technol.*, 2010, **44**, 6614–6620.
26 R. Oswald, T. Behrendt, M. Ermel, D. Wu, H. Su, Y. Cheng, C. Breuninger, A. Moravek, E. Mougin, C. Delon, B. Loubet, A. Pommerening-Roser, M. Sorgel, U. Poschl, T. Hoffmann, M. O. Andreae, F. X. Meixner and I. Trebs, *Science*, 2013, **341**, 1233–1235.
27 P. Di Carlo, W. H. Brune, M. Martinez, H. Harder, R. Lesher, X. R. Ren, T. Thornberry, M. A. Carroll, V. Young, P. B. Shepson, D. Riemer, E. Apel and C. Campbell, *Science*, 2004, **304**, 722–725.
28 Y. Nakashima, S. Kato, J. Greenberg, P. Harley, T. Karl, A. Turnipseed, E. Apel, A. Guenther, J. Smith and Y. Kajii, *Atmos. Environ.*, 2014, **85**, 1–8.
29 Y. Sadanaga, A. Yoshino, S. Kato and Y. Kajii, *Environ. Sci. Technol.*, 2005, **39**, 8847–8852.
30 A. Yoshino, Y. Nakashima, K. Miyazaki, S. Kato, J. Suthawaree, N. Shimo, S. Matsunaga, S. Chatani, E. Apel, J. Greenberg, A. Guenther, H. Ueno, H. Sasaki, J. Hoshi, H. Yokota, K. Ishii and Y. Kajii, *Atmos. Environ.*, 2012, **49**, 51–59.
31 A. C. Nolscher, J. Williams, V. Sinha, T. Custer, W. Song, A. M. Johnson, R. Axinte, H. Bozem, H. Fischer, N. Pouvesle, G. Phillips, J. N. Crowley, P. Rantala, J. Rinne, M. Kulmala, D. Gonzales, J. Valverde-Canossa, A. Vogel, T. Hoffmann, H. G. Ouwersloot, J. V. G. de Arellano and J. Lelieveld, *Atmos. Chem. Phys.*, 2012, **12**, 8257–8270.
32 D. R. Hanson, J. Greenberg, B. E. Henry and E. Kosciuch, *Int. J. Mass Spectrom.*, 2003, **223**, 507–518.
33 J. J. Colman, A. L. Swanson, S. Meinardi, B. C. Sive, D. R. Blake and F. S. Rowland, *Anal. Chem.*, 2001, **73**, 3723–3731.
34 NIER, *Development of the Asia Emission Inventory in Support of Integrated Modeling of Climate and Air Quality*, National Institute of Environmental Research, Incheon, South Korea, 2013.
35 I. Bey, D. J. Jacob, R. M. Yantosca, J. A. Logan, B. D. Field, A. M. Fiore, Q. B. Li, H. G. Y. Liu, L. J. Mickley and M. G. Schultz, *J. Geophys. Res.: Atmos.*, 2001, **106**, 23073–23095.
36 R. J. Park, D. J. Jacob, M. Chin and R. V. Martin, *J. Geophys. Res.: Atmos.*, 2003, **108**.
37 R. J. Park, D. J. Jacob, B. D. Field, R. M. Yantosca and M. Chin, *J. Geophys. Res.: Atmos.*, 2004, **109**.
38 H. Liao, D. K. Henze, J. H. Seinfeld, S. L. Wu and L. J. Mickley, *J. Geophys. Res.: Atmos.*, 2007, **112**.
39 H. O. T. Pye, H. Liao, S. Wu, L. J. Mickley, D. J. Jacob, D. K. Henze and J. H. Seinfeld, *J. Geophys. Res.: Atmos.*, 2009, **114**.

40 A. B. Guenther, X. Jiang, C. L. Heald, T. Sakulyanontvittaya, T. Duhl, L. K. Emmons and X. Wang, *Geosci. Model Dev.*, 2012, **5**, 1471–1492.
41 Q. Zhang, D. G. Streets, G. R. Carmichael, K. B. He, H. Huo, A. Kannari, Z. Klimont, I. S. Park, S. Reddy, J. S. Fu, D. Chen, L. Duan, Y. Lei, L. T. Wang and Z. L. Yao, *Atmos. Chem. Phys.*, 2009, **9**, 5131–5153.
42 G. R. van der Werf, J. T. Randerson, L. Giglio, G. J. Collatz, M. Mu, P. S. Kasibhatla, D. C. Morton, R. S. DeFries, Y. Jin and T. T. van Leeuwen, *Atmos. Chem. Phys.*, 2010, **10**, 11707–11735.
43 T. Ohara, H. Akimoto, J. Kurokawa, N. Horii, K. Yamaji, X. Yan and T. Hayasaka, *Atmos. Chem. Phys.*, 2007, **7**, 4419–4444.
44 J. H. Woo, S. He, E. Tagaris, K. J. Liao, K. Manomaiphiboon, P. Amar and A. G. Russell, *J. Air Waste Manage. Assoc.*, 2008, **58**, 1483–1494.
45 S. W. Kim, A. Heckel, S. A. McKeen, G. J. Frost, E. Y. Hsie, M. K. Trainer, A. Richter, J. P. Burrows, S. E. Peckham and G. A. Grell, *Geophys. Res. Lett.*, 2006, **33**.
46 K. D. Lu, A. Hofzumahaus, F. Holland, B. Bohn, T. Brauers, H. Fuchs, M. Hu, R. Haseler, K. Kita, Y. Kondo, X. Li, S. R. Lou, A. Oebel, M. Shao, L. M. Zeng, A. Wahner, T. Zhu, Y. H. Zhang and F. Rohrer, *Atmos. Chem. Phys.*, 2013, **13**, 1057–1080.
47 M. Shao, S. H. Lu, Y. Liu, X. Xie, C. C. Chang, S. Huang and Z. M. Chen, *J. Geophys. Res.: Atmos.*, 2009, **114**.
48 X. Tie, F. Geng, A. Guenther, J. Cao, J. Greenberg, R. Zhang, E. Apel, G. Li, A. Weinheimer, J. Chen and C. Cai, *Atmos. Chem. Phys.*, 2013, **13**, 5655–5669.
49 X. Tie, G. Brasseur and Z. Ying, *Atmos. Chem. Phys.*, 2010, **10**, 8983–8995.
50 T. M. S. S. Comittee, *Megacity Air Pollution Studies-Seoul (MAPS-Seoul)*, National Institute of Environmental Research, 2015.
51 T. K.-A. S. Group, *NASA Contributions to KORUS-AQ: In International Cooperative Air Quality Field Study in Korea*, NASA, 2015.
52 W. Y. Xu, C. S. Zhao, L. Ran, W. L. Lin, P. Yan and X. B. Xu, *Atmos. Chem. Phys.*, 2014, **14**, 7757–7768.
53 K. H. Kim, D. X. Ho, C. G. Park, C. J. Ma, S. K. Pandey, S. C. Lee, H. J. Jeong and S. H. Lee, *Environ. Eng. Sci.*, 2012, **29**, 875–889.
54 C. Warneke, S. A. McKeen, J. A. de Gouw, P. D. Goldan, W. C. Kuster, J. S. Holloway, E. J. Williams, B. M. Lerner, D. D. Parrish, M. Trainer, F. C. Fehsenfeld, S. Kato, E. L. Atlas, A. Baker and D. R. Blake, *J. Geophys. Res.: Atmos.*, 2007, **112**.
55 R. Atkinson, D. L. Baulch, R. A. Cox, J. N. Crowley, R. F. Hampson, R. G. Hynes, M. E. Jenkin, M. J. Rossi and J. Troe, *Atmos. Chem. Phys.*, 2006, **6**, 3625–4055.
56 L. Ran, C. S. Zhao, W. Y. Xu, M. Han, X. Q. Lu, S. Q. Han, W. L. Lin, X. B. Xu, W. Gao, Q. Yu, F. H. Geng, N. Ma, Z. Z. Deng and J. Chen, *Atmos. Chem. Phys.*, 2012, **12**, 7531–7542.
57 W. L. Chameides, F. C. Fehsenfeld, M. O. Rodgers, C. Cadelino, J. Martinez, D. D. Parrish, W. Loneman, D. R. Lawson, R. Rasmusse, P. Zimmerman, J. Greenberg, P. Middleton and T. Wang, *J. Geophys. Res.*, 1992, **97**, 6037–6055.
58 S. Kim, A. Guenther, T. Karl and J. Greenberg, *Atmos. Chem. Phys.*, 2011, **11**, 8613–8623.
59 M. Ehn, J. A. Thornton, E. Kleist, M. Sipila, H. Junninen, I. Pullinen, M. Springer, F. Rubach, R. Tillmann, B. Lee, F. Lopez-Hilfiker, S. Andres, I. H. Acir, M. Rissanen, T. Jokinen, S. Schobesberger, J. Kangasluoma,

J. Kontkanen, T. Nieminen, T. Kurten, L. B. Nielsen, S. Jorgensen, H. G. Kjaergaard, M. Canagaratna, M. Dal Maso, T. Berndt, T. Petaja, A. Wahner, V. M. Kerminen, M. Kulmala, D. R. Worsnop, J. Wildt and T. F. Mentel, *Nature*, 2014, **506**, 476.

60 T. Jokinen, T. Berndt, R. Makkonen, V. M. Kerminen, H. Junninen, P. Paasonen, F. Stratmann, H. Herrmann, A. Guenther, D. R. Worsnop, M. Kulmala, M. Ehn and M. Sipila, *Proc. Natl. Acad. Sci. U. S. A.*, 2015, **112**, 7123–7128.

61 T. Zhu, M. Melamed, D. Parrish, M. Gauss, L. G. Klenner, M. G. Lawrence, A. Konare and C. Liousse, *WMO/IGAC Impacts of Megacities on Air Pollution and Climate*, Geneva, Switzerland, 2012.

62 Y. Wang, M. H. Wang, R. Y. Zhang, S. J. Ghan, Y. Lin, J. X. Hu, B. W. Pan, M. Levy, J. H. Jiang and M. J. Molina, *Proc. Natl. Acad. Sci. U. S. A.*, 2014, **111**, 6894–6899.

63 J. W. Fan, D. Rosenfeld, Y. Yang, C. Zhao, L. R. Leung and Z. Q. Li, *Geophys. Res. Lett.*, 2015, **42**, 6066–6075.

64 D. T. Shindell, G. Faluvegi, D. M. Koch, G. A. Schmidt, N. Unger and S. E. Bauer, *Science*, 2009, **326**, 716–718.